Technical Report

TR-05-19

Probabilistic analysis of canister inserts for spent nuclear fuel

Peter Dillström, Det Norske Veritas

October 2005

Svensk Kärnbränslehantering AB
Swedish Nuclear Fuel
and Waste Management Co
Box 5864
SE-102 40 Stockholm Sweden
Tel 08-459 84 00
+46 8 459 84 00
Fax 08-661 57 19
+46 8 661 57 19

Probabilistic analysis of canister inserts for spent nuclear fuel

Peter Dillström, Det Norske Veritas

October 2005

Summary

In this study, probabilistic analysis of canister inserts for spent nuclear fuel has been performed. The main conclusions are:

1. For the baseline case, the probability of failure is insignificant ($\sim 2\times10^{-9}$). This is the case even though several conservative assumptions have been made both in underlying deterministic analysis and in the probabilistic analysis.
2. The initiation event dominates (over the local collapse event) when the external pressure is below the baseline case (p = 44 MPa). The local collapse event dominates when the external pressure is above the baseline case.
3. The local collapse event is strongly dependent of the assumed external pressure.
4. The analysis of collapse only considers the first local collapse event, total collapse of the insert will occur at a much higher pressure.
5. The resulting probabilities are more dependent on the assumption regarding the eccentricity of the cassette than the assumption regarding outer corner radius of the profiles for steel section cassette. The results indicate that the maximum allowed eccentricity should not be larger than 5 mm.
6. The probability of initiation of crack growth is calculated using a defect distribution where one assumes the existence of one crack-like defect. A simple scaling argument can be applied to consider the number of defects through the thickness.

Contents

1 Introduction

Nuclear waste in Sweden is handled by the Swedish Nuclear Fuel and Waste Management Co, SKB. Several decades of research and development has led SKB to put forward the KBS-3 method for the final stage of the spent nuclear fuel management. In this method, copper canisters with a cast iron insert containing spent nuclear fuel are surrounded by bentonite clay and deposited at approximately 500 m depth in saturated, granitic rock, see Figure 1-1.

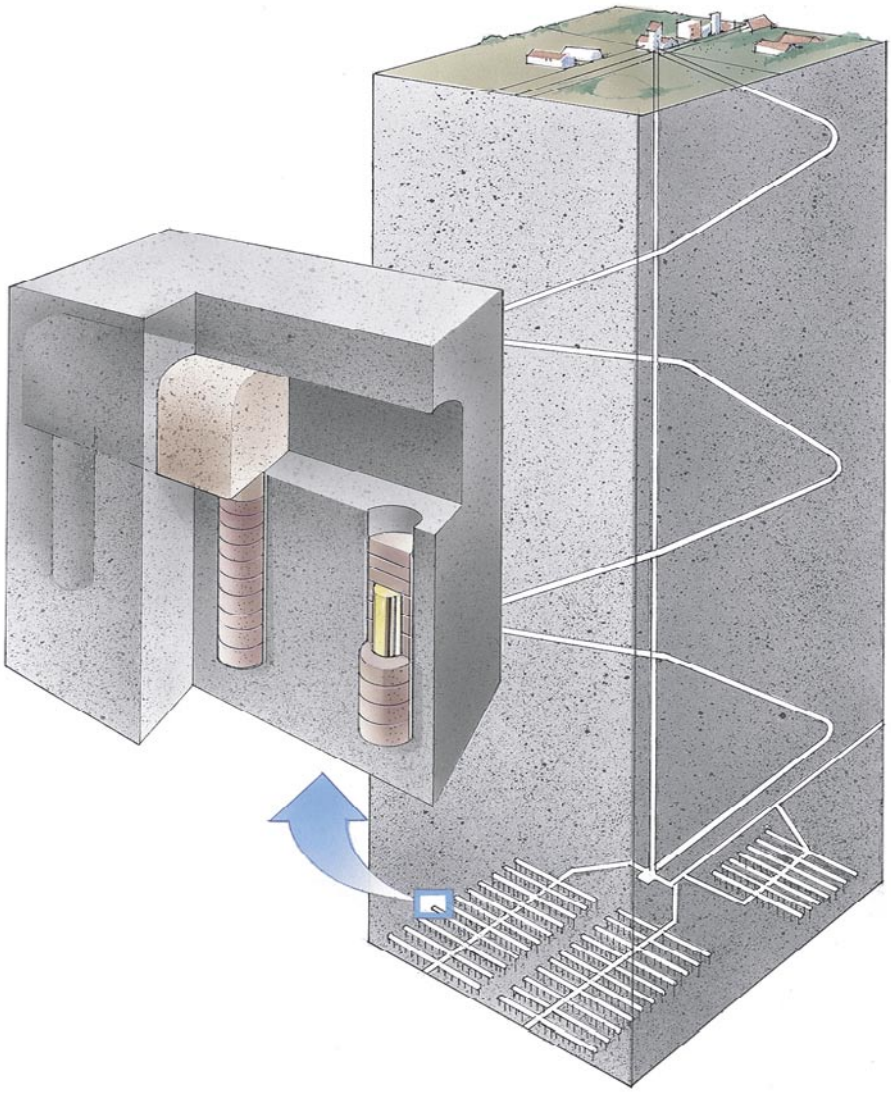

Figure 1-1. *SKB is going to build a deep repository for all spent nuclear fuel.*

The primary safety function of the KBS 3 system is to completely isolate the spent nuclear fuel within copper canisters over the entire assessment period. Should a canister be damaged, the secondary safety function is to retard any releases from the canisters. The two issues of isolation and retardation are thus in focus throughout the assessment.

The canister consists of a pressure-bearing insert of nodular iron with a steel lid, Figure 1-2. The insert contains channels for the fuel assemblies, 12 in the BWR version and 4 in the PWR version. The insert is surrounded by an outer corrosion barrier of copper. In the repository the canisters will be loaded in compression by the hydrostatic pressure and the swelling pressure from the surrounding bentonite, giving a total pressure of 14 MPa. During the extreme time scales, several ice ages are expected with a maximum ice-sheet of 3 km resulting in an additional pressure of 30 MPa. The maximum design pressure for the KBS-3 canisters has therefore been assumed to be 44 MPa.

For the licensing procedures of depositories for spent nuclear fuel safety analyses are performed. Among other items it is required to obtain an estimate of the probability of mechanical failure of canisters even by considering the effects of a possible ice age. At the end of 2002 a project was initiated to obtain such an estimate. Different activities such as material testing, stress and strain calculations, full-scale testing as well as probabilistic analyses have been conducted by different organisations. In the present report the probabilistic analysis of canister inserts for spent nuclear fuel is summarised.

Figure 1-2. *Canister for final depository of spent nuclear fuel.*

2 Parameters to be included in the analysis

When performing a probabilistic analysis of the canister inserts, the important parameters that influence the calculated failure probabilities should be identified. Within this project it was decided that the following parameters should be considered.

Material data

- Fracture toughness (K_{Ic},J_{Ic}).
- Yield stress in tension ($R_{p0.2}^{Tension}$).
- Ultimate strength in tension ($R_{m}^{Tension}$).
- Yield stress in compression ($R_{p0.2}^{Compression}$).
- Ultimate strength in compression ($R_{m}^{Compression}$).
- Strain to be used in the material model definition ($\varepsilon_{failure}$).

Geometry and defects

- Outer corner radius of the profiles for steel section cassette (r_{corner}).
- Eccentricity of the cassette ($\delta_{cassette}$).
- Defect distribution (f_a).

Loading

- External pressure (p).

These parameters are described in more detail below.

2.1 Fracture toughness

Fracture toughness testing has been performed by the department of solid mechanics (KTH) /1–2/, and also by JRC /3/. The tests were performed using three-point bend specimens at different temperatures (between 0°C and 100°C). The following remarks were made /1–4/.

- In all cases the fracture mechanics tests exhibited ductile behaviour with rising J_r curves. In the probabilistic analysis, only initiation values are used. The calculated probabilities will therefore be quite conservative because of the assumed failure mode without any consideration of stable crack growth.
- Slightly different results were achieved at different temperatures and also for different inserts (inserts I24, I25 and I26 were tested).
- There was no significant difference between specimens taken from the bottom and upper slab, neither between specimens taken from the transverse or longitudinal directions.
- The results presented by JRC are somewhat lower than the results presented by KTH. At present there is no explanation to why this difference occurs.

Comparing the room temperature results from JRC and KTH shows that the JRC results are more conservative and will therefore be used in the probabilistic analysis. In the analysis one uses K_{Ic}-data (instead of the presented J_{Ic}-data /3/) given as $K_{Ic} = \sqrt{J_{Ic} E / \left(1-\nu^2\right)}$, where E = 172 GPa /5/ and ν = 0.3.

Data to be used in the probabilistic analysis:

- Fracture toughness (mean value) = 83.5 MPa $\sqrt{\text{m}}$.
- Fracture toughness (standard deviation) = 11.8 MPa $\sqrt{\text{m}}$.
- Fracture toughness distribution = Normal /6/.

2.2 Yield stress and ultimate strength in tension

JRC and the Swedish Foundry Association performed tensile tests on 50 specimens from each of the three inserts I24, I25 and I26. The yield stress, the ultimate tensile strength and the elongation after fracture were determined. The results from JRC and the Swedish Foundry Association were very consistent with respect to the mean and standard deviation of yield stress, ultimate tensile strength and elongation after fracture and also to systematic variation between different inserts and locations of specimen. A summary of test results and a statistical analysis of these data are given in /7/.

The large variations in the results are quite remarkable, especially for the elongation. Insert I25 has a significantly higher failure strain than specimens from inserts I24 and I26 and the specimens from the bottom slab have a higher failure strain. However, the tensile curves measured by JRC were more or less identical until fracture occurs. This observation suggested that the fracture process was controlled by the nature and size of the defect(s) present in the specimen tested /4/.

However, stress analysis of the insert shows that the resulting stresses and strains are independent of the assumptions made, regarding yield stress and ultimate strength in tension, in the analysis. This is also true for the probabilistic analysis; the probability of initiation of crack growth and probability of local collapse are independent of the assumed values of yield stress and ultimate strength in tension. It was therefore decided to use the more relevant compression data for the failure mode “local collapse” also when calculating the probability of initiation of crack growth. Another possible approach would be to treat this data as being deterministic, but then the probabilistic model has to be somewhat redefined.

Data to be used in the probabilistic analysis:

- See the compression data below.

2.3 Yield stress and ultimate strength in compression

JRC and Kockums AB performed compression tests on a few specimens from each of the three inserts I24, I25 and I26 /8–9/. Kockums were only able to produce yield stress values. JRC did produce both yield stress and ultimate compression strength values. The compression test data delivered by JRC exhibited very small variations, which was expected since such data are not controlled by defects /4/.

The six data points from JRC are used in the analysis (the only available data for this study). Yield stress data is taken directly from /9/, ultimate strength data is taken from the curve fits given in /9/ for a true strain of 10% (as defined in Section 2.4 below).

Data to be used in the probabilistic analysis:

- Yield stress in compression (mean value) = 270 MPa.
- Yield stress in compression (standard deviation) = 6 MPa.
- Ultimate strength in compression (mean value) = 478 MPa.
- Ultimate strength in compression (standard deviation) = 6 MPa.
- Yield stress distribution = Normal /6/.
- Ultimate compression strength distribution = Normal /6/.

2.4 Strain to be used in the material model definition

As input data for the probabilistic analysis, several deterministic stress analyses of the insert are needed. In these calculations a simplified bilinear elastic-plastic material model and the ANSYS finite element software are used /10–11/. The bilinear material model is defined using an elastic modulus (up to the yield stress, for the elastic part) and a tangent modulus (for the plastic part). The tangent modulus is, somewhat arbitrary, defined using the ultimate strength value at 10% true strain.

Doing a sensitivity analysis, with a complete stress strain curve, shows that this simplification is conservative and that the differences in the results are quite small (up to an applied external pressure of 100 MPa).

2.5 Outer corner radius of the profiles for steel section cassette

In the manufacturing of the inserts, the outer corner radius, r_{corner}, of the profiles for steel section cassette (see Figure 2-1) has a tolerance that allows for a variation of the radius between 15 and 25 mm. This has an influence on the stresses close to the corner, but also on the ligament stresses (because a smaller corner radius has a negative influence on the wall thickness).

Within this study, it was decided to treat this parameter deterministically. How the radius influence the calculated probabilities are therefore shown using different sensitivity studies as shown in Section 4.

Data to be used in the probabilistic analysis:

- r_{corner} = 15, 20, 25 mm.

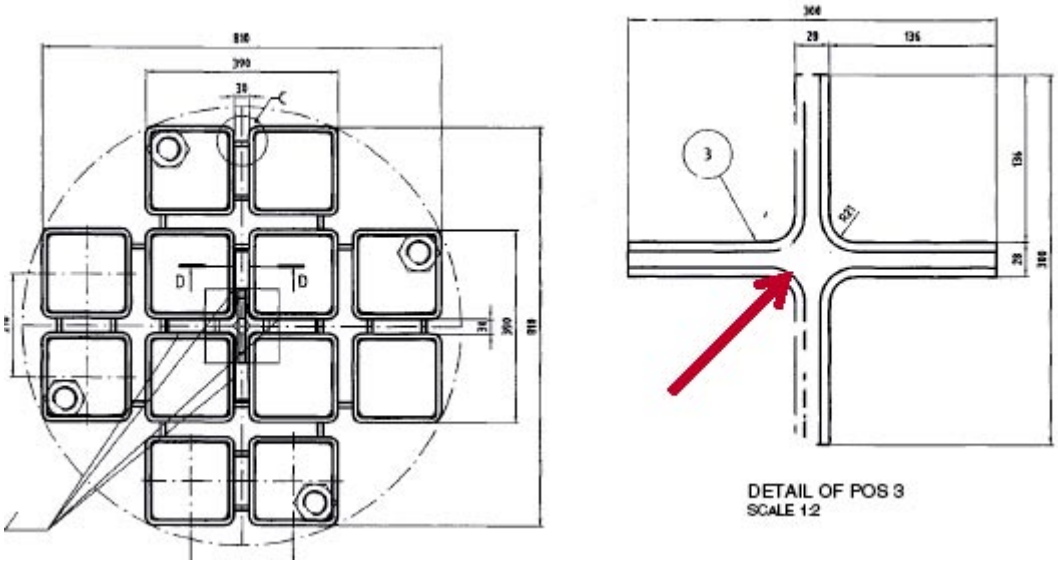

Figure 2-1. *Outer corner radius, r_{corner}, of the profiles for steel section cassette /12/.*

2.6 Eccentricity of the cassette

In the manufacturing of the inserts, there is a possibility that the steel section cassette will have an offset relative to the centre of the insert (see Figure 2-2). Within this study, we call this the eccentricity of the cassette, $\delta_{cassette}$. The eccentricity has an influence on the ligament stresses (because a smaller corner radius has a negative influence on the wall thickness).

The eccentricity, as shown in Figure 2-2, was measured to be 12 mm, which is very large. As part of this study, SKB has recently decided that there should be a tolerance that allows for a variation of the eccentricity between 0 and 5 mm.

In the present study, it was decided to treat this parameter deterministically. How the eccentricity influence the calculated probabilities are therefore shown using different sensitivity studies as shown in Section 4.

Data to be used in the probabilistic analysis:

- $\delta_{cassette}$ = 0, 5, 10, 15 mm.

2.7 Defect distribution

As stated in Section 2.2, the results from the tensile tests showed large variations regarding the failure strain and ultimate tensile strength. The conclusion was that the relevant fracture process was controlled by the nature and size of the defect(s) present in the specimen tested /4/. When calculating the probability of initiation of crack growth, one therefore has to include a defect size distribution.

JRC has conducted an extensive fractographic and metallographic study on broken specimens to check for defects /14/. This was done by first performing a detailed and unbiased analysis for a number of specimens to screen for defects or microstructural imperfections that might cause low failure strain. As indicated in Figure 2-3, there is a clear trend that the failure strain decreases with increasing defect size.

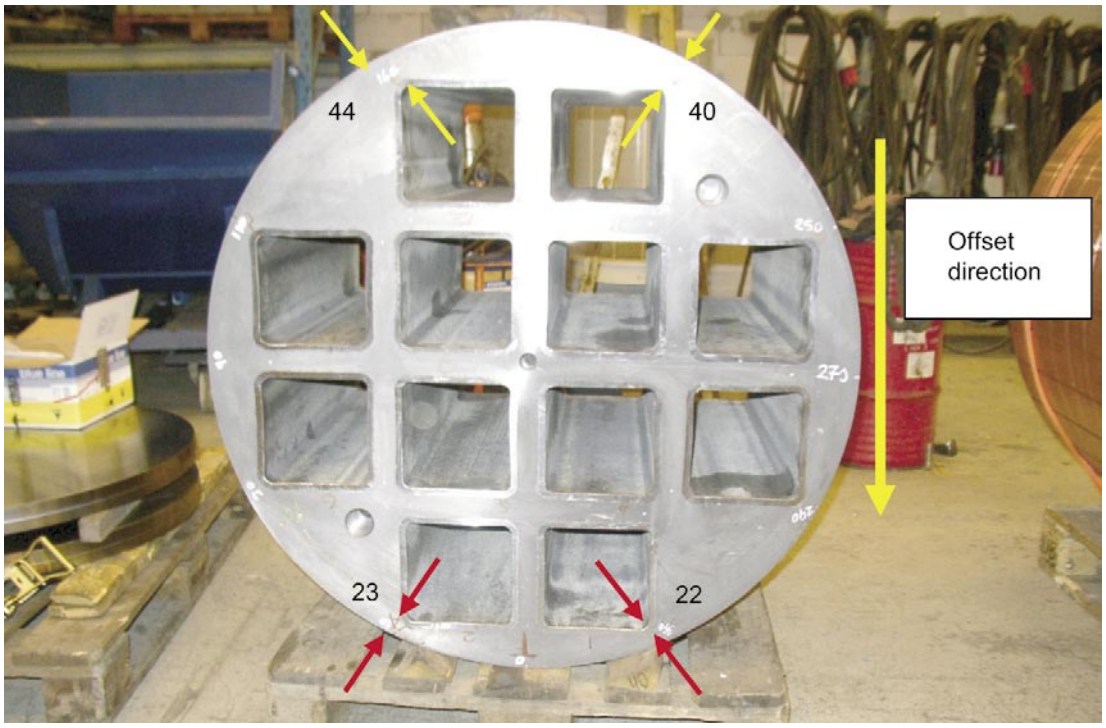

Figure 2-2. *Example with a large final eccentricity of the steel section cassette /13/.*

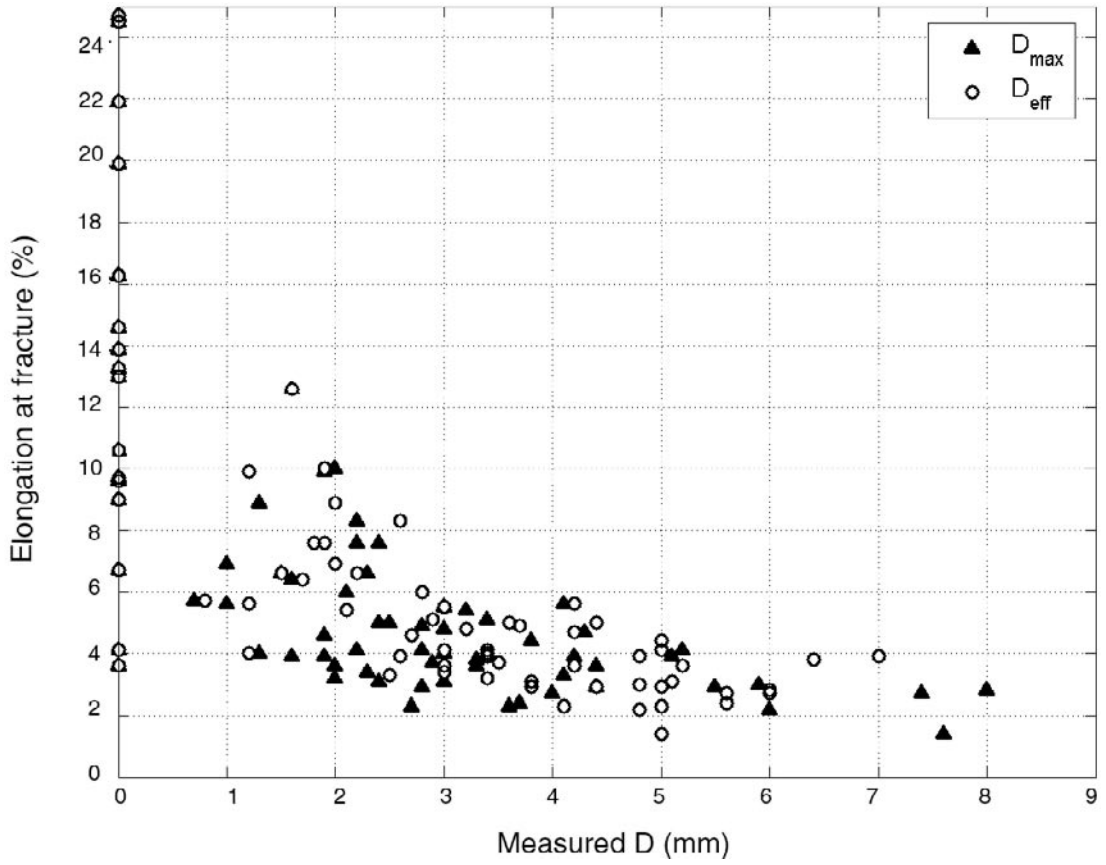

Figure 2-3. *The measured failure strain versus measured size of defects.*

A probabilistic model, that can be used to derive different defect distributions, was developed by JRC /14/. The model assumes the existence of one crack-like defect, and the size of this defect is characterised by an exponential distribution. Using different model assumptions (with and without a truncation of the failure strain) and data from the inserts I24 and I26, different exponential defect distributions were derived. The mean value of these distributions was estimated between 0.7 and 1.9 mm. In the probabilistic analysis, it is conservative to use an upper estimate. In order to simplify the analysis we assume that the defect is surface breaking, which is more severe than a subsurface defect and therefore conservative.

Data to be used in the probabilistic analysis:

- Defect geometry = a semi-elliptical surface defect.
- Defect length/depth = 6.
- Defect depth (mean value) = 1.9 mm.
- Defect distribution = Exponential /14/ (the JRC model assumes the existence of one crack-like defect, a simple scaling argument can be applied to consider the number of defects through the thickness).

2.8 External pressure

In the repository the canisters will be loaded in compression by the hydrostatic pressure and the swelling pressure from the surrounding bentonite, giving a total assumed pressure of 14 MPa. During the extreme time scales, several ice ages are expected with a maximum ice-sheet of 3 km resulting in an additional pressure of 30 MPa. The maximum design pressure for the KBS-3 canisters has therefore been assumed to be 44 MPa.

A large number of Finite Element stress analyses /15/, with aid of the software ANSYS /10–11/, were performed in order to provide input to the probabilistic analysis. It was decided to include an external pressure up to 60 MPa in these calculations.

Data to be used in the probabilistic analysis:

- External pressure = 0, 15, 25, 35, 40, 45, 50, 60 MPa.

3 Deterministic stress analysis

A large number of Finite Element stress analyses /15/, with aid of the software ANSYS /10–11/, were performed in order to provide input to the probabilistic analysis. Since the amount of computational work was very large, the bulk of the analyses were performed on simplified two-dimensional models. In order to verify the relevance of this idealisation a comparison with full three-dimensional analysis was conducted. The results of this comparison showed that the two-dimensional computations gave satisfactory accurate results.

Also, in order to simplify the analysis, geometric symmetry showed that only 1/8 of the insert needed to be included in the finite element model (see Figure 3-1). Finally, the steel cassette and the outer corrosion barrier made of copper was not included in the model (a sensitivity analysis validated that this was a conservative idealisation). The resulting finite element model is shown in Figure 3-2 (using r_{corner} = 20 mm and $\delta_{cassette}$ = 0 mm).

The stress calculations were made using a simplified bilinear elastic-plastic material model. The bilinear material model is defined using an elastic modulus (up to the yield stress, for the elastic part) and a tangent modulus (for the plastic part). The tangent modulus is, somewhat arbitrary, defined using the ultimate strength value at 10% true strain (see Section 2.4).

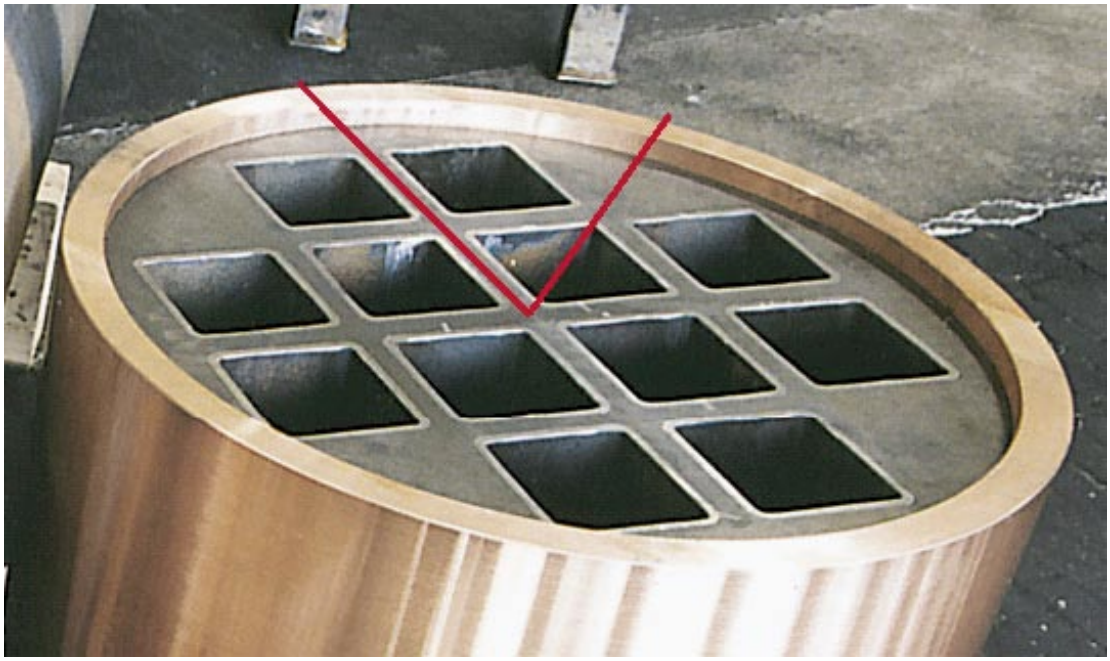

Figure 3-1. *Insert with symmetry lines that was used in finite element idealisation.*

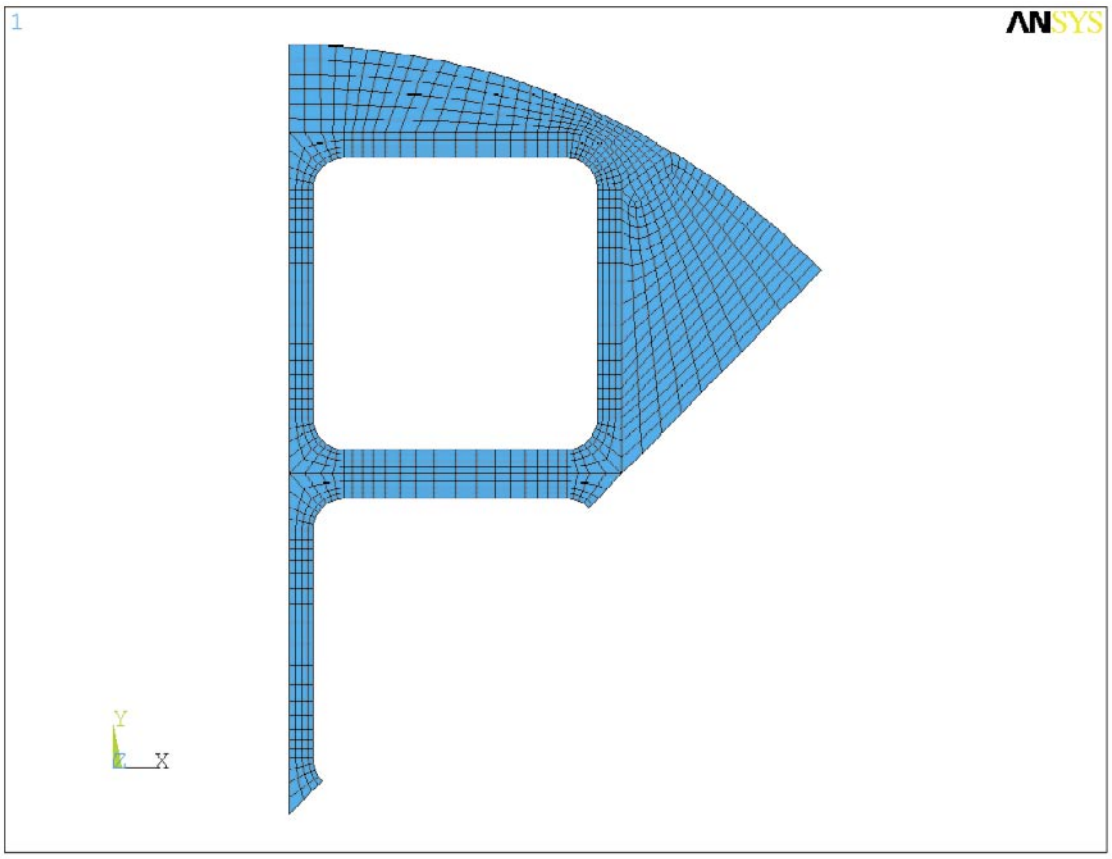

Figure 3-2. *Finite element model used in the stress analysis (example using rcorner = 20 mm and* $\delta_{cassette}$ *= 0 mm).*

From the base model, variations of the following parameters of the model were made.

- Influence of the outer corner radius (r_{corner}) of the profiles for steel section cassette.
- Influence of the eccentricity of the steel cassette ($\delta_{cassette}$). This influence was simulated by changing the outer radius of the canister.
- Influence of change of the material properties i.e. yield stress ($R_{p0.2}^{Compression}$) and ultimate strength ($R_m^{Compression}$) in compression.

The total parameter matrix (the number of model combinations/analyses were 300) is summarised in Table 3-1.

In all cases the stress state of the insert was mainly compressive (see Section 3.1), but there was also a region with tensile stresses at the fuel channel facing the outside of the insert (see Section 3.2). The size of the region with tensile stresses increased with the applied pressure and also increased as the corner radius became smaller or as the eccentricity became larger.

The maximum effective stress is shown as function of the external pressure for different corner radius and for different eccentricities (in Figures 3-3 and 3-4, respectively) /15/.

As indicated in Figures 3-3 and 3-4, the insert has an elastic behaviour up to an external pressure of 15 MPa. Local collapse of the ligament (at the fuel channel facing the outside of the insert) begins at an external pressure of approximately 50 MPa (40 MPa if $\delta_{cassette}$ = 15 mm).

Table 3-1. Parameter matrix for the deterministic stress analysis.

Parameter	Variable	Index	Number	1	2	3	4	5	Unit
Outer radius	r_{outer}	1	4	474.5	469.5	464.5	459.5		mm
Corner radius	r_{corner}	2	3	15	20	25			mm
Yield stress	$R_{p0.2}$	3	5	200	250	270	290	350	MPa
Ultimate strength	R_m	4	5	400	450	475	500	550	MPa
Total number of combinations (analyses)			300						

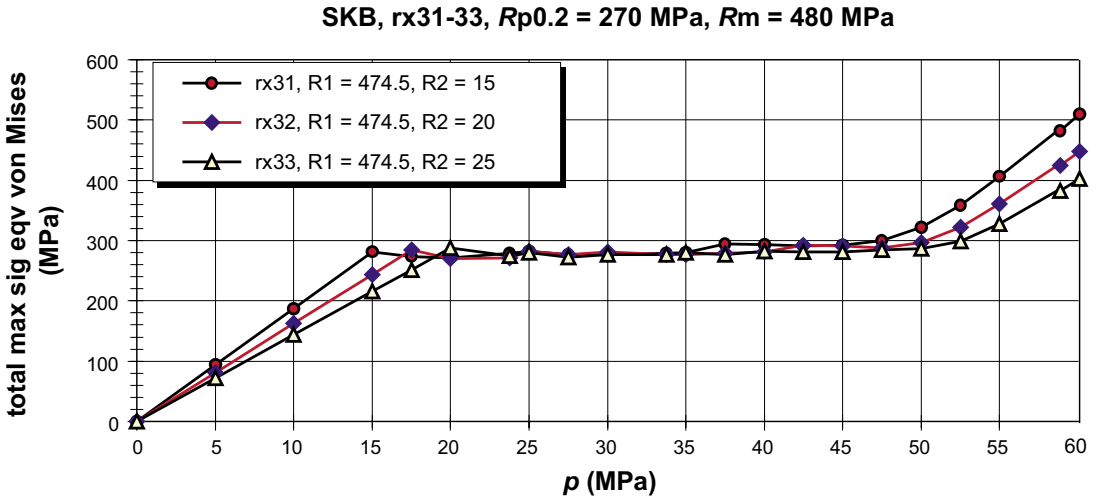

Figure 3-3. *Maximum effective stress, as a function of the external pressure, for different values of the corner radius (using mean values of yield stress and ultimate strength in compression) /15/.*

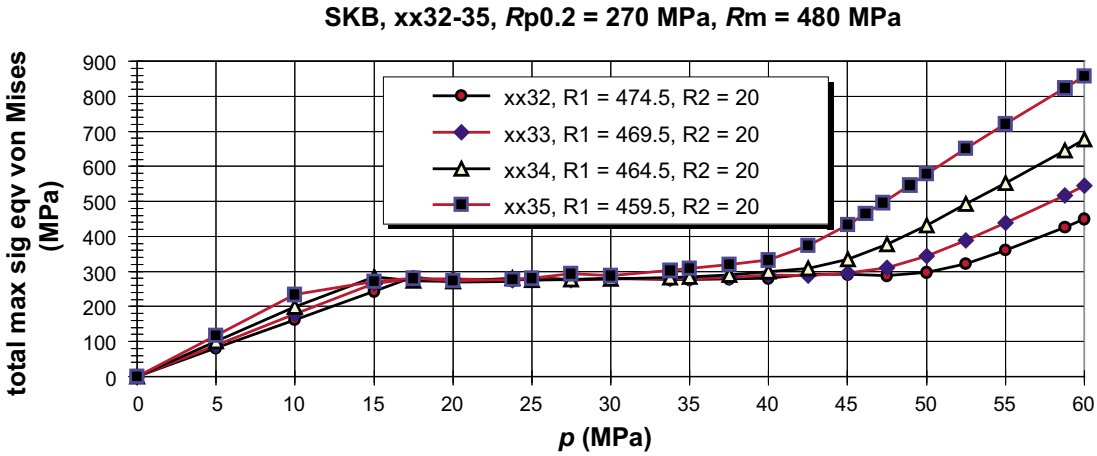

Figure 3-4. *Maximum effective stress, as a function of the external pressure, for different values of the eccentricity (using mean values of yield stress and ultimate strength in compression) /15/.*

3.1 Stress distribution – analysis of plastic collapse

In all cases the stress state of the insert was mainly compressive and when the external pressure is below ~ 30 MPa a stress concentration (in compression) dominates the stress field at the fuel channel facing the outside of the insert (see Figure 3-5). However, as the external pressure increases, also the plastic flow increases until a local collapse of the ligament occurs (see Figure 3-6). The dominating parameters that control the local collapse are the applied external pressure and the eccentricity of the steel cassette (see Figure 3-4).

The stress component that is most interesting, regarding a local collapse of the ligament, is related to the largest principal stress in compression (see Figure 3-7). This is the stress component that follows the corner radius and therefore perpendicular to a path through the thickness (starting at the stress/strain concentration at the corner).

The stress component perpendicular to a path through the thickness will therefore be used as input to the probabilistic analysis. Several other paths were also evaluated and typical examples are shown in Figure 3-8.

The probabilistic analysis of plastic collapse only considers the initial local collapse of the ligament. This is a conservative assumption since the final collapse of the insert will be at a much higher external pressure. The final collapse geometry (collapse analysis using ANSYS) is shown in Figure 3-9.

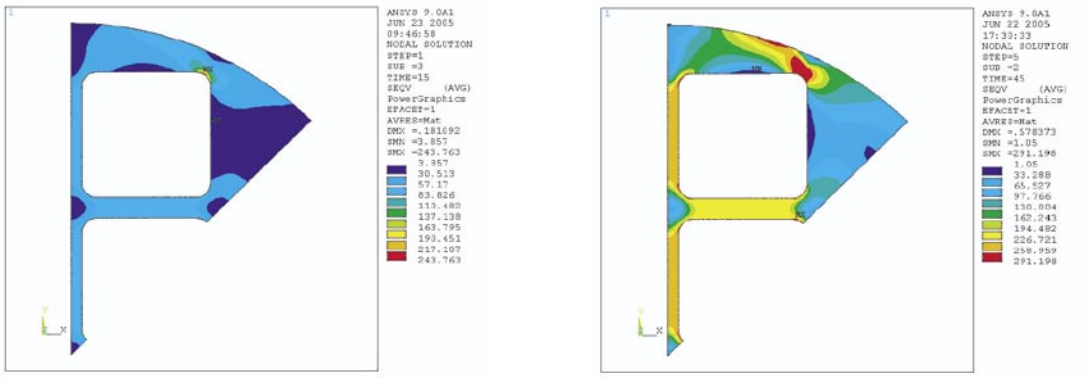

Figure 3-5. *Effective stresses when p = 15 MPa (left plot) and p = 45 MPa (right plot). Results using r_{corner} = 20 mm, $\delta_{cassette}$= 0 mm and mean material data.*

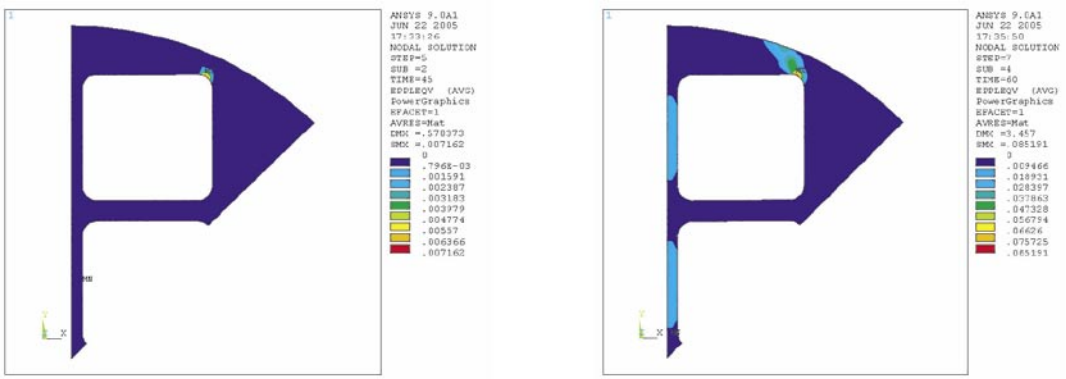

Figure 3-6. *Effective plastic strains when p = 45 MPa (left plot) and p = 60 MPa (right plot). Results using r_{corner} = 20 mm, $\delta_{cassette}$ = 0 mm and mean material data.*

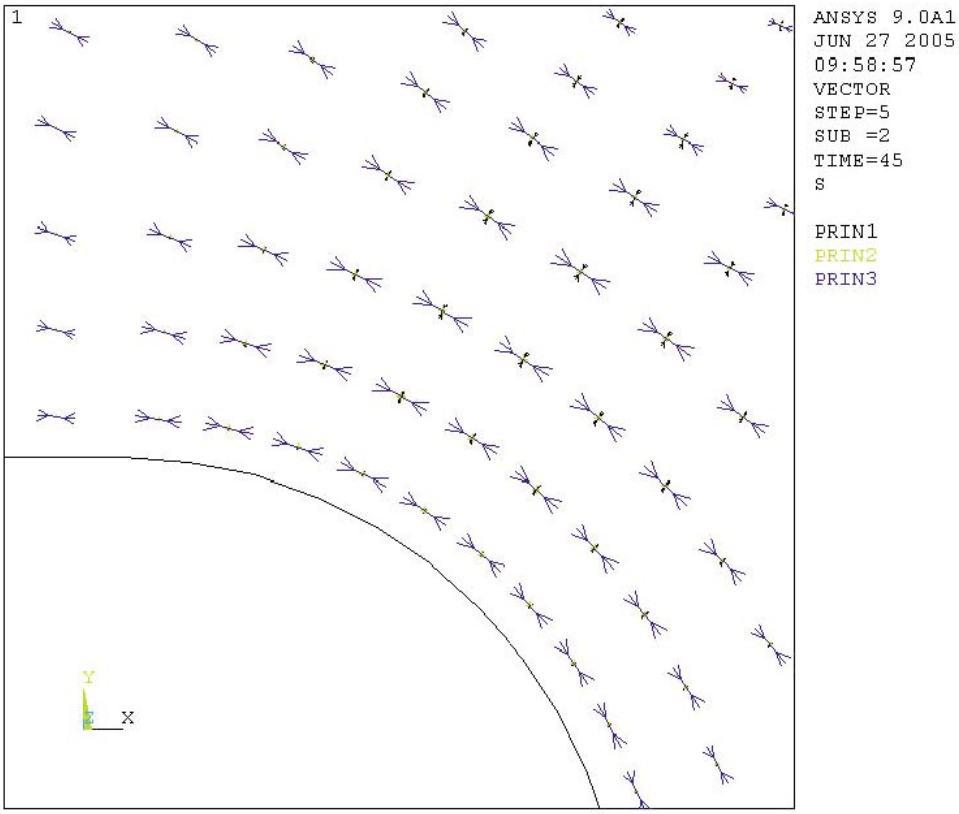

Figure 3-7. *Principal stresses close to the corner radius. The largest principal stress in compression is* σ_3 *(PRIN3 in the plot).*

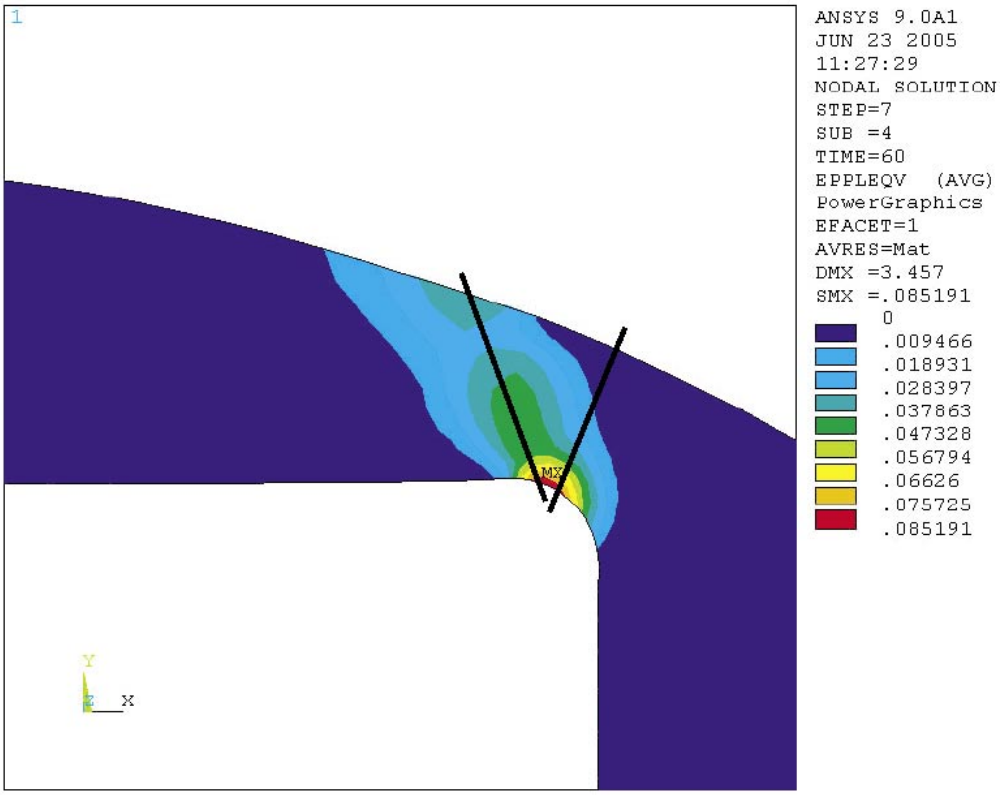

Figure 3-8. *Examples of two paths that have been used to generate stress input to the probabilistic analysis.*

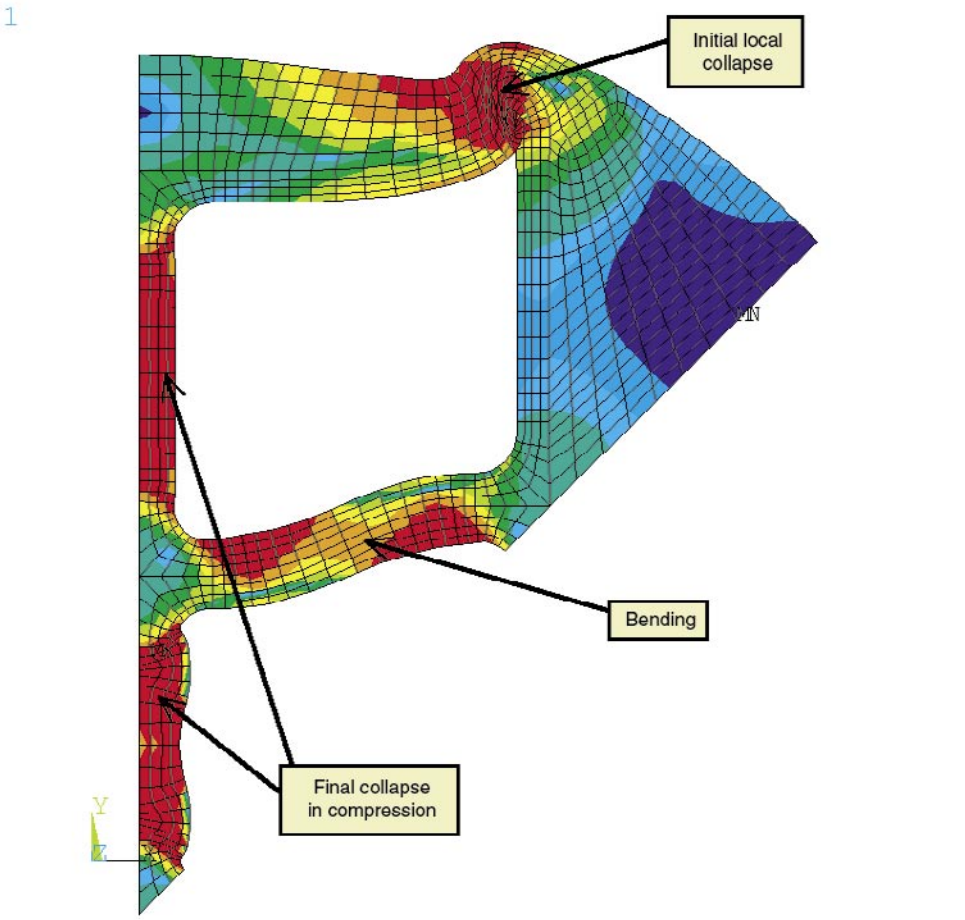

Figure 3-9. *Final collapse geometry (collapse analysis using ANSYS, plot of the effective stress at the final collapse pressure).*

3.2 Stress distribution – analysis of initiation of crack growth

As already stated above, the stress state of the insert was mainly compressive, but there was also a region with tensile stresses at the fuel channel facing the outside of the insert (see Figure 3-10). The size of the region with tensile stresses increased with the applied pressure and also increased as the corner radius became smaller or as the eccentricity became larger.

The stress component that is most interesting, regarding initiation of crack growth, is related to the principal stress (σ_1) which could be in tension (see Figure 3-10). The largest principal stress is located within the material (when the external pressure is below ~ 45 MPa) or at the inner surface (when the external pressure is above ~ 45 MPa or when $\delta_{cassette}$ is larger than ~ 5 mm).

The principal stress (σ_1) along a path through the thickness will therefore be used as input to the probabilistic analysis. Several paths were evaluated and typical examples are shown in Figure 3-11.

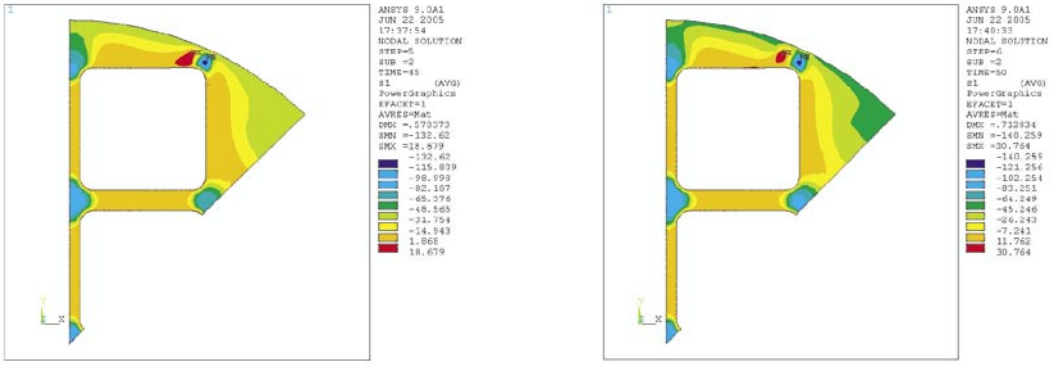

Figure 3-10. *Principal stress (σ_1) when p = 45 MPa (left plot) and p = 50 MPa (right plot). Results using r_{corner} = 20 mm, $\delta_{cassette}$ = 0 mm and mean material data.*

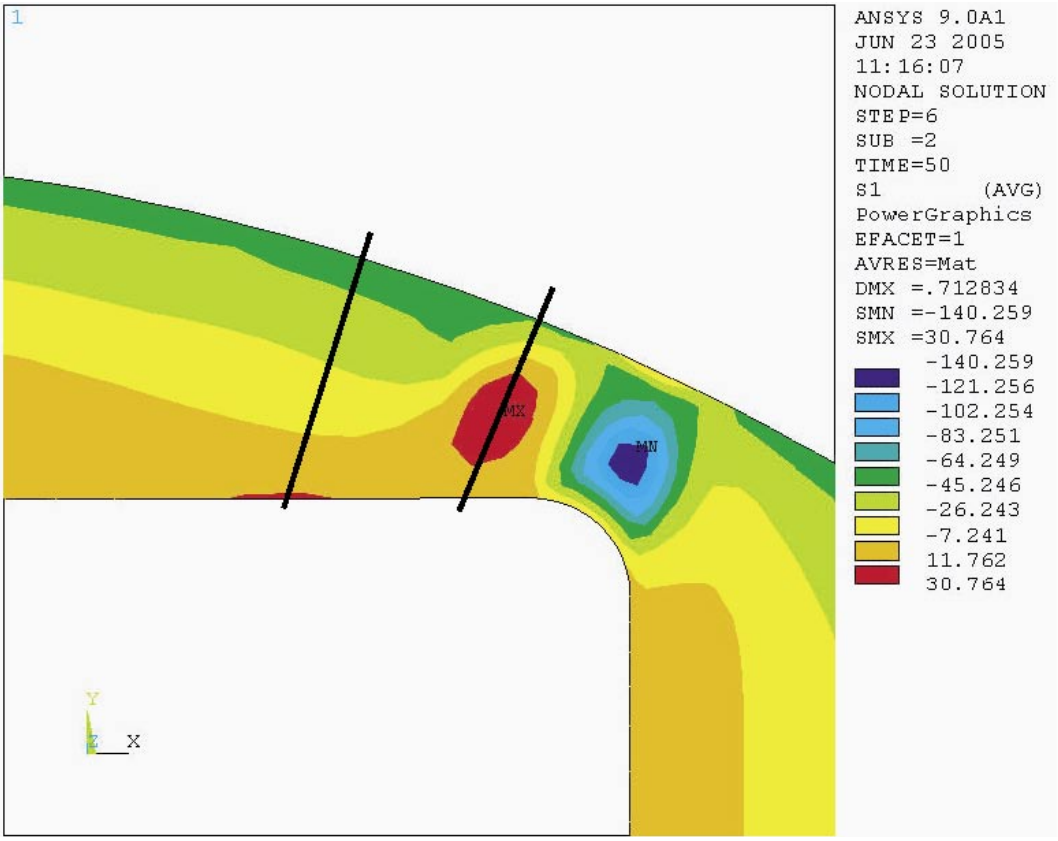

Figure 3-11. *Examples of two paths that have been used to generate stress input to the probabilistic analysis.*

Examples of principal stresses along a typical path are found in Figure 3-12 (using r_{corner} = 20 mm and $\delta_{cassette}$ = 0 mm). As shown in the figure, the largest principal stress is located within the material in this case. If r_{corner} = 15 mm, the stresses will be slightly larger and if r_{corner} = 25 mm, the stresses will be smaller.

Examples of principal stresses along a typical path are found in Figure 3-13 (using r_{corner} = 20 mm and $\delta_{cassette}$ = 10 mm). As shown in the figure, the largest principal stress is located at the inner surface in this case. If $\delta_{cassette}$ > 5 mm, then the tensile stresses at the inner surface will be very large (i.e. the probability of initiation of crack growth will also be large).

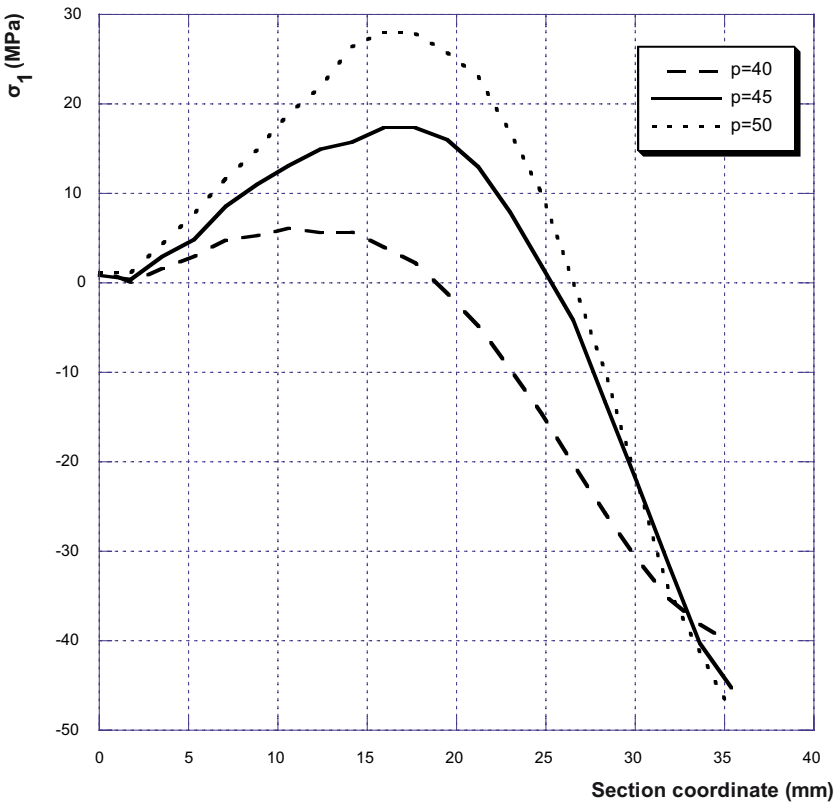

Figure 3-12. *Principal stress (σ_1) when p = 40–50 MPa. Results using r_{corner} = 20 mm, $\delta_{cassette}$ = 0 mm and mean material data.*

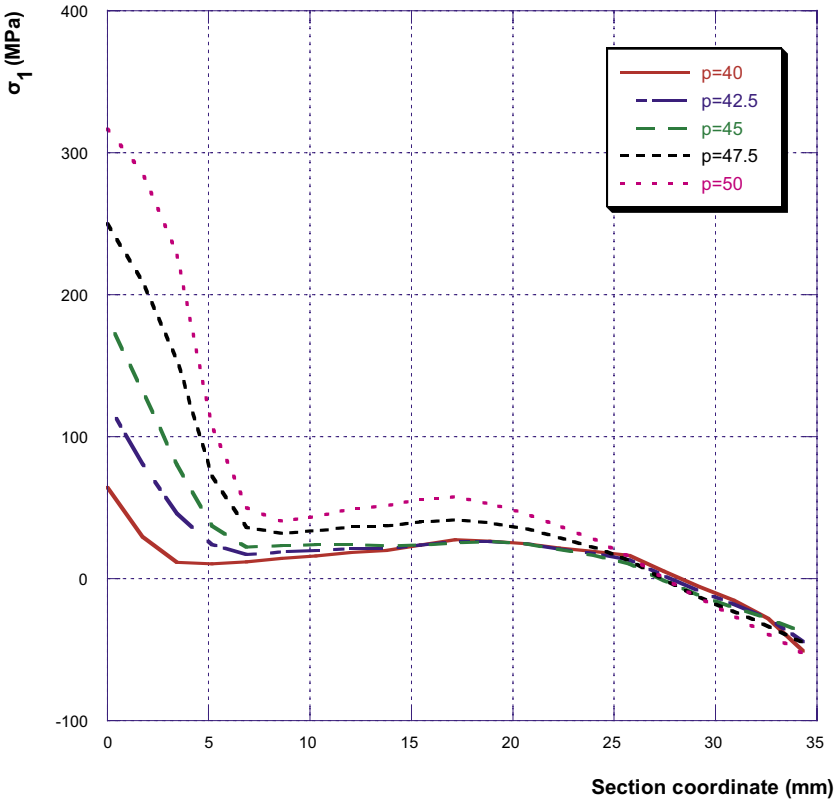

Figure 3-13. *Principal stress (σ_1) when p = 40–50 MPa. Results using r_{corner} = 20 mm, $\delta_{cassette}$ = 10 mm and mean material data.*

4 Probabilistic analysis

Using the input data as given in Section 2 (fracture toughness, yield stress in tension/ compression, ultimate strength in tension/compression, outer corner radius of the profiles for steel section cassette, eccentricity of the cassette, defect distribution, external pressure) and Section 3 (stresses), it is then possible to calculate the probability of a local plastic collapse of the ligament and the probability of initiation of crack growth.

4.1 Theoretical background

Before presenting the results from the probabilistic analysis, a theoretical background is given below /6/. In this report, two different probabilities are calculated:

- Probability of local plastic collapse.
- Probability of initiation of crack growth, defect not detected by NDT/NDE.

The underlying procedure /6/ uses two different limit state functions, $g(X)$ ($g_{FAD}(X)$ and $g_{L_r^{max}}(X)$).

$$g_{FAD}(X) = f_{FAD}(X) - K_r(X) \quad \text{(initiation of crack growth),} \tag{4.1}$$

$$g_{L_r^{max}}(X) = L_r^{\max}(X) - L_r(X) \quad \text{(plastic collapse).} \tag{4.2}$$

These limit state functions are based on a simplified R6 failure assessment curve /6/. To calculate the probability of failure, a multi-dimensional integral has to be evaluated /6/:

$$P_F = \Pr[g(X) < 0] = \int_{g(X)<0} f_X(x)dx \quad . \tag{4.3}$$

The set where the above analysed event is fulfilled, is formulated as $g(X) < 0$, and is called the failure set. The set where $g(X) > 0$ is called the safe set. $f_X(x)$ is a known joint probability density function of the random vector X. This integral is very hard (impossible) to evaluate, by numerical integration, if there are many random parameters. The random parameters (as given in Section 2) are treated as not being correlated with one another.

As mentioned above, the failure probability integral is very hard to solve using numerical integration. Instead, the following numerical algorithms are included within the procedure /6/:

- Simple Monte Carlo Simulation (MCS).
- First-Order Reliability Method (FORM).

Simple Monte Carlo Simulation (MCS)

MCS is a simple method that uses the fact that the failure probability integral can be interpreted as a mean value in a stochastic experiment. An estimate is therefore given by averaging a suitably large number of independent outcomes (simulations) of this experiment.

The basic building block of this sampling is the generation of random numbers from a uniform distribution (between 0 and 1). Simple algorithms "repeats themselves" (already) after approximately 2×10^3 to 2×10^9 simulations and are therefore not suitable to calculate medium to small failure probabilities. The algorithm chosen within the procedure repeats itself after approx. 2×10^{18} simulations. This algorithm is approximately 20 times slower than the simpler algorithms mentioned above, but it is recommended if one needs more than 1×10^8 simulations.

Once a random number u, between 0 and 1, has been generated, it can be used to generate a value of the desired random variable with a given distribution. A common method is the inverse transform method. Using the cumulative distribution function $F_X(x)$, the random variable would then be given as:

$$x = F_X^{-1}(u) \quad . \tag{4.4}$$

To calculate the failure probability, one performs N deterministic simulations and for every simulation checks if the component analysed has failed (i.e. if $g(X) < 0$). The number of failures is N_F, and an estimate of the mean probability of failure is:

$$P_{F,MCS} = \frac{N_F}{N} \quad . \tag{4.5}$$

An advantage with MCS, is that it is robust and easy to implement into a computer program, and for a sample size $N \to \infty$, the estimated probability converges to the exact result. Another advantage is that MCS works with any distribution of the random variables and there is no restriction on the limit state functions.

However, MCS is inefficient when calculating failure probabilities, since most of the contribution to P_F is in a limited part of the integration interval.

First/Second-Order Reliability Method (FORM/SORM)

FORM/SORM uses a combination of both analytical and approximate methods, when estimating the probability of failure.

First, one transforms all the variables into equivalent normal variables in standard normal space (i.e. with mean = 0 and standard deviation = 1). This means that the original limit state surface $g(x) = 0$ then becomes mapped onto the new limit state surface $g_U(u) = 0$.

Secondly, one calculates the shortest distance between the origin and the limit state surface (in a transformed standard normal space U). The answer is a point on this surface, and it is called the most probable point of failure (MPP), design point or β-point. The distance between the origin and the MPP is called the reliability index β_{HL} (see Figure 4-1).

In general, it requires an appropriate non-linear optimisation algorithm to calculate the most probable point of failure. However, a linearization of the limit state function is commonly used to calculate the MPP.

$$y_{i+1} = \frac{1}{\left|\nabla g_U(y_i)\right|^2} \cdot \left[\nabla g_U(y_i) \cdot y_i - g_U(y_i)\right] \cdot \nabla g_U(y_i)^T \quad , \tag{4.6}$$

where y_i is the current approximation to the MPP and $\nabla g_U(y_i)$ is the gradient of the limit state function. This algorithm, generally called the Rackwitz & Fiessler (R & F) algorithm, is commonly used when evaluating P_F, mainly because it is very easy to implement and it converges fast in many cases. However, the R & F algorithm converges extremely slowly in

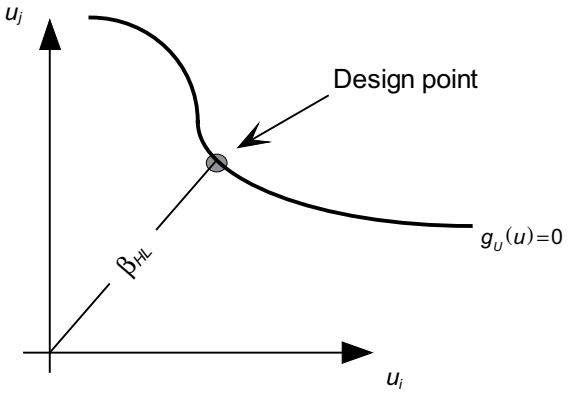

Figure 4-1. *The definition of design point/MPP and reliability index* β_{HL}.

some cases or oscillates about the solution without any convergence at all. In the procedure /6/ both of these problems occur when $P_F > 0.8$ or when $P_F < 10^{-7}$ (also between these values in some cases). Therefore, the R & F algorithm was not chosen in the procedure /6/.

In the procedure, a modified Rackwitz & Fiessler algorithm was chosen. It works by "damping" the gradient contribution of the limit state function and this algorithm is very robust and converges quite fast for most cases. In this algorithm one defines a search direction vector d_i:

$$d_i = \frac{1}{\left|\nabla g_U(y_i)\right|^2} \cdot \left[\nabla g_U(y_i) \cdot y_i - g_U(y_i)\right] \cdot \nabla g_U(y_i)^T - y_i \quad . \tag{4.7}$$

A new approximation to the MPP can then be calculated:

$$y_{i+1} = y_i + s_i \cdot d_i \quad . \tag{4.8}$$

The step size s_i was selected such that the inequality $m(y_i + s_i d_i) < m(y_i)$ holds, where $m(y_i)$ is the merit function:

$$m(y_i) = \frac{1}{2} \cdot \left|y_i\right|^2 + c \cdot \left|g_U(y_i)\right| \quad , \tag{4.9}$$

in which c is a parameter satisfying the condition $c > \left|y_i\right| / \left|\nabla g_U(y_i)\right|$ at each step i. This algorithm is globally convergent, i.e. the sequence is guaranteed to converge to a minimum-distance point on the limit state surface, provided $g_U(u)$ is continuous and differentiable.

Finally, one calculates the failure probability using an approximation of the limit state surface at the most probable point of failure. Using FORM, the surface is approximated to a hyperplane (a first order/linear approximation). SORM uses a second order/quadratic approximation to a hyperparaboloid (see Figure 4-2).

The probability of failure is given as:

$$P_{F,FORM} = \Pr\left[g_{Linear}(u) < 0\right] = \Phi(-\beta_{HL}) \quad , \tag{4.10}$$

$$P_{F,SORM} = \Pr\left[g_{Quadratic}(u) < 0\right] \approx \Phi(-\beta_{HL}) \cdot \prod_{i=1}^{N-1} \left(1 - \kappa_i \cdot \beta_{HL}\right)^{-1/2} \quad , \tag{4.11}$$

where $\Phi(u)$ is the cumulative distribution function in standard normal space and κ_i are the principal curvatures of the limit state surface at the most probable point of failure (MPP).

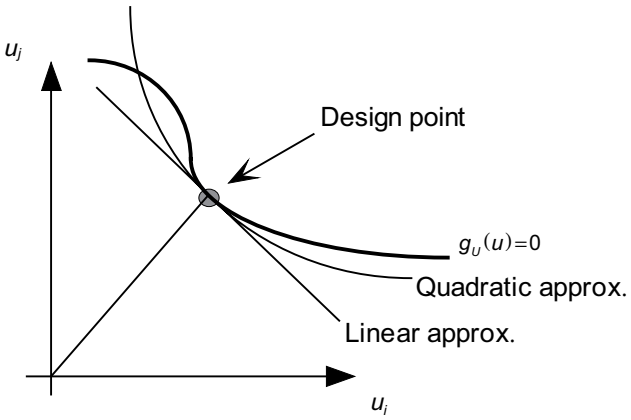

Figure 4-2. *Schematic difference between a linear and a quadratic approximation of the limit state surface.*

FORM/SORM are, as regards CPU-time, extremely efficient as compared to MCS. Using the FORM implementation within the procedure, you get quite accurate results for failure probabilities between 10^{-1} to 10^{-15}. A disadvantage is that the random parameters must be continuous, and every limit state function must also be continuous.

4.2 Probability of local plastic collapse

The probability of plastic collapse is independent of the chosen defect distribution (because the collapse mode is in compression). Using the procedure in Section 4.1 and the data given in Section 2 and 3, the probability of plastic collapse is estimated to be $P_{collapse} = 1.40 \times 10^{-21}$ (using $p = 44$ MPa, $r_{corner} = 20$ mm, $\delta_{cassette} = 0$ mm).

Sensitivity analysis (as a function of the applied external pressure) using different outer corner radius of the profiles for steel section cassette (r_{corner}) and eccentricity of the cassette ($\delta_{cassette}$) are presented in Figures 4-3 and 4-4.

As shown in Figures 4-3 and 4-4, the parameters "applied external pressure" and "eccentricity of the cassette" has the strongest influence on the results. If $\delta_{cassette}$ is larger than ~ 5–10 mm, then the probability of plastic collapse is very large (if $p = 44$ MPa).

The results presented in Figures 4-3 and 4-4 are also summarised in Table 4-1.

In this study, the amount of tensile tests (more than one hundred data points according to Section 2.2) was much larger than the amount of compression tests (six data points according to Section 2.3). Therefore, it would be interesting to check the assumption regarding variation of the yield stress and ultimate strength in compression. The base line assumption is that the standard deviation is 6 MPa (using the six data points in compression). The result from this sensitivity study is presented in Figure 4-5 below.

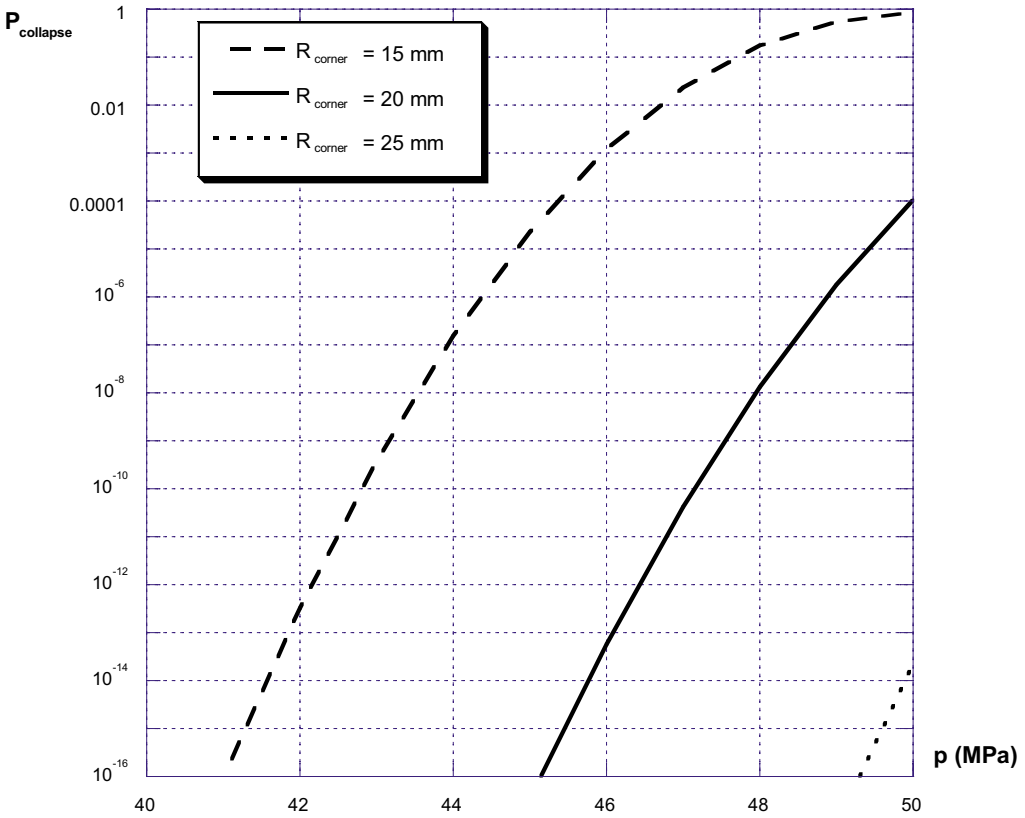

Figure 4-3. *Probability of plastic collapse when p = 40–50 MPa. Results using r_{corner} = 15–25 mm, $\delta_{cassette}$ = 0 mm.*

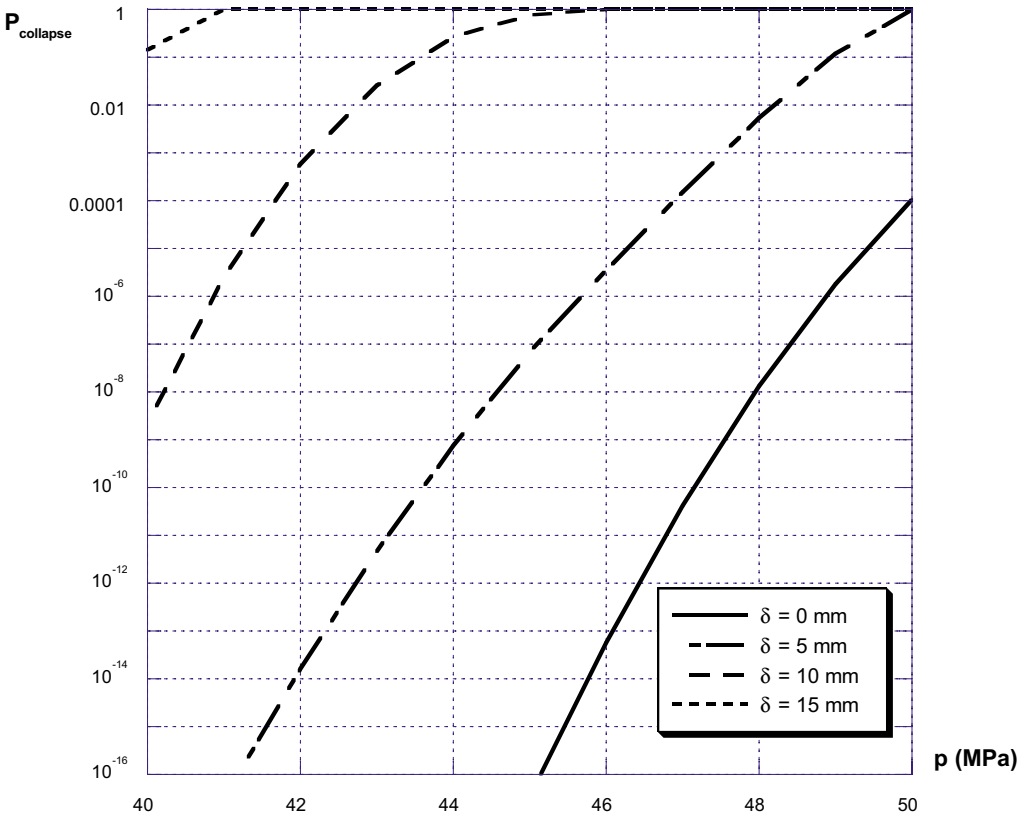

Figure 4-4. *Probability of plastic collapse when p = 40–50 MPa. Results using r_{corner} = 20 mm, $\delta_{cassette}$ = 0–15 mm.*

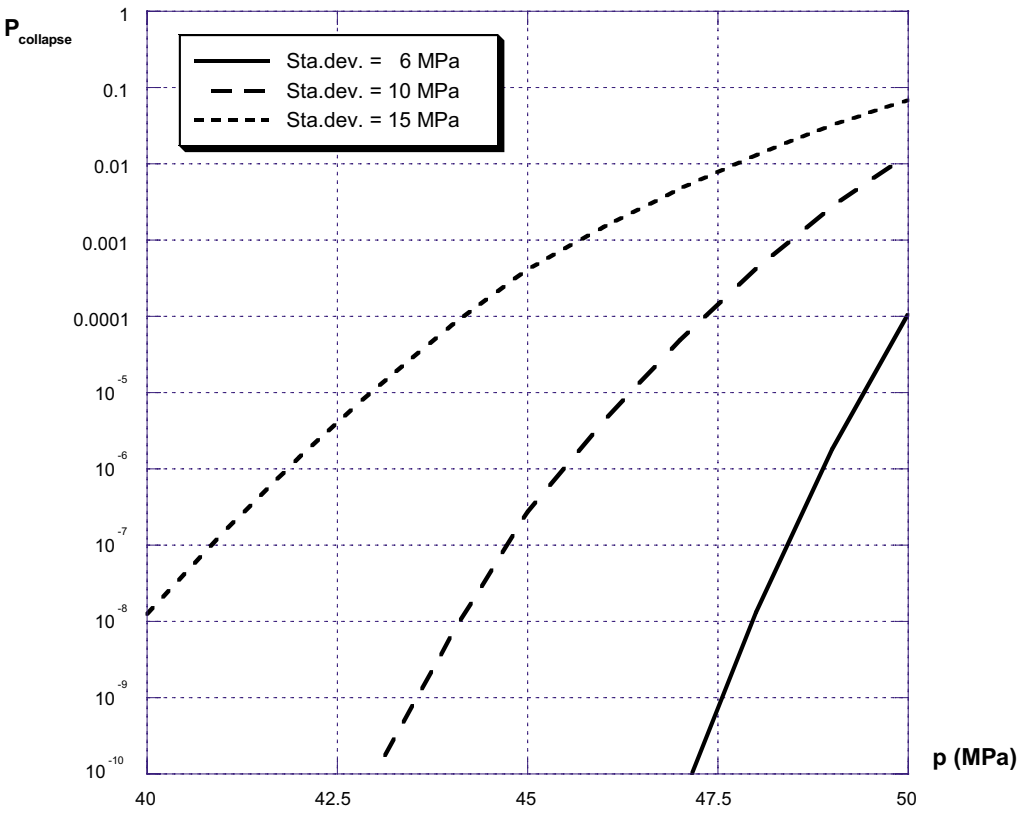

Figure 4-5. *Probability of plastic collapse when p = 40–50 MPa. Results using r_{corner} = 20 mm, $\delta_{cassette}$ = 0 mm, standard deviation ($R_{p0.2}^{Compression}$, $R_m^{Compression}$) = 6–15 MPa.*

Table 4-1. Probability of plastic collapse when *p* = 40–50 MPa. Results using r_{corner} = 15–25 mm and $\delta_{cassette}$ = 0–15 mm.

		$\delta_{cassette}$ = 0	$\delta_{cassette}$ = 5	$\delta_{cassette}$ = 10	$\delta_{cassette}$ = 15
	r_{corner} = 15	1.13×10^{-20}	–	–	–
p = 40	r_{corner} = 20	1.96×10^{-44}	3.78×10^{-20}	2.28×10^{-9}	0.142
	r_{corner} = 25	$< 1\times10^{-50}$	–	–	–
	r_{corner} = 15	1.56×10^{-7}			
p = 44	r_{corner} = 20	1.40×10^{-21}	7.53×10^{-10}	0.264	1.00
	r_{corner} = 25	2.39×10^{-41}			
	r_{corner} = 15	2.30×10^{-5}	–	–	–
p = 45	r_{corner} = 20	3.47×10^{-17}	6.85×10^{-8}	0.751	1.00
	r_{corner} = 25	7.37×10^{-35}	–	–	–
	r_{corner} = 15	0.877	–	–	–
p = 50	r_{corner} = 20	1.09×10^{-4}	1.00	1.00	1.00
	r_{corner} = 25	2.28×10^{-14}	–	–	–

Note: Empty cells represent combinations that were not part of the sensitivity study.

4.3 Probability of initiation of crack growth

4.3.1 Probability of initiation of crack growth from one defect

Using the procedure in Section 4.1 and the data given in Section 2 and 3, the probability of initiation of crack growth is estimated to be $P_{initiation} = 7.57 \times 10^{-13}$ (using $p = 44$ MPa, $r_{corner} = 20$ mm, $\delta_{cassette} = 0$ mm).

Sensitivity analysis (as a function of the applied external pressure) using different outer corner radius of the profiles for steel section cassette (r_{corner}) and eccentricity of the cassette ($\delta_{cassette}$) are presented in Figures 4-6 and 4-7.

As shown in Figures 4-6 and 4-7, the parameters "applied external pressure" and "eccentricity of the cassette" has the strongest influence on the results. If $\delta_{cassette}$ is larger than ~ 10–15 mm, then the probability of initiation of crack growth is very large (if $p =$ 44 MPa).

The results presented in Figures 4-6 and 4-7 are also summarised in Table 4-2.

In this study, the mean value of the defect depth distribution was estimated between 0.7 and 1.9 mm. It would be interesting to check this assumption (especially for larger assumed defect depths). The result from this sensitivity study is presented in Figure 4-8 below.

As seen in Figure 4-8, the resulting probability is rather insensitive to the assumed mean value of the defect depth distribution.

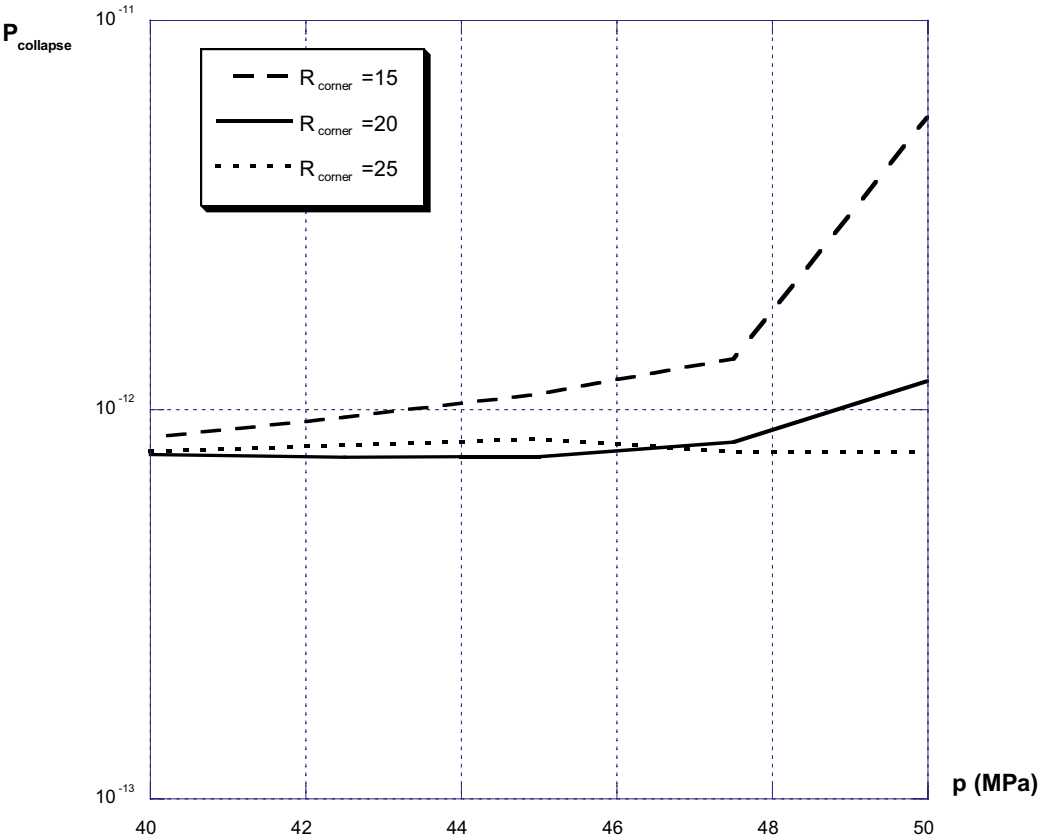

Figure 4-6. *Probability of initiation of crack growth when p = 40–50 MPa. Results using r_{corner} = 15–25 mm, $\delta_{cassette}$ = 0 mm, μ_a = 1.9 mm.*

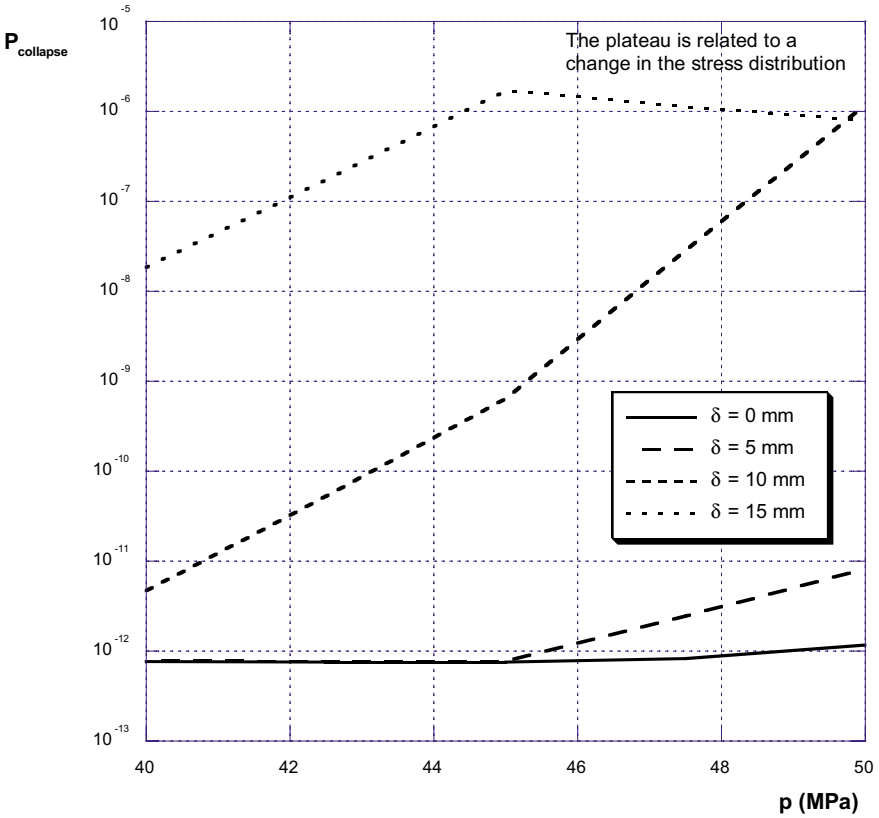

Figure 4-7. *Probability of initiation of crack growth when p = 40–50 MPa. Results using r_{corner} = 20 mm, $\delta_{cassette}$ = 0–15 mm, μ_a = 1.9 mm.*

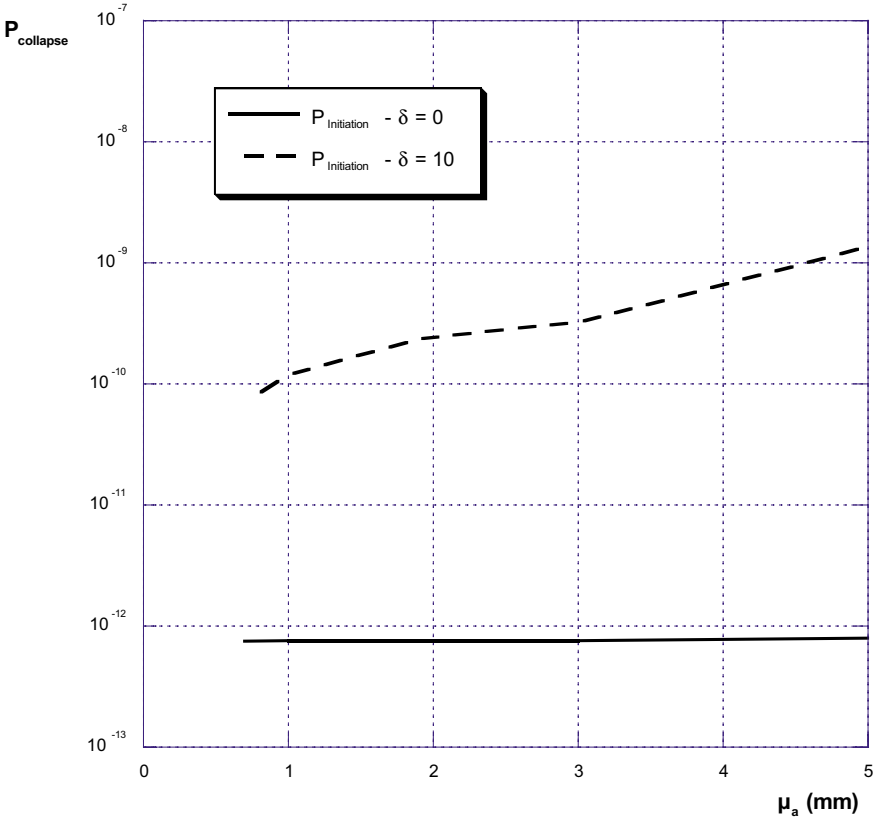

Figure 4-8. *Probability of initiation of crack growth when p = 44 MPa. Results using r_{corner} = 20 mm, $\delta_{cassette}$ = 0–10 mm, μ_a = 0.7–5 mm.*

Table 4-2. Probability of initiation of crack growth when p = 40–50 MPa. Results using r_{corner} = 15–25 mm, $\delta_{cassette}$ = 0–15 mm and μ_a = 1.9 mm.

		$\delta_{cassette}$ = 0	$\delta_{cassette}$ = 5	$\delta_{cassette}$ = 10	$\delta_{cassette}$ = 15
	r_{corner} = 15	8.48×10^{-13}	–	–	–
p = 40	r_{corner} = 20	7.68×10^{-13}	7.84×10^{-13}	4.73×10^{-12}	1.84×10^{-8}
	r_{corner} = 25	7.83×10^{-13}	–	–	–
	r_{corner} = 15	1.04×10^{-12}	–	–	–
p = 44	r_{corner} = 20	7.57×10^{-13}	7.79×10^{-13}	2.36×10^{-10}	6.80×10^{-7}
	r_{corner} = 25	8.27×10^{-13}	–	–	–
	r_{corner} = 15	1.10×10^{-12}	–	–	–
p = 45	r_{corner} = 20	7.59×10^{-13}	7.78×10^{-13}	6.37×10^{-10}	1.69×10^{-6}
	r_{corner} = 25	8.38×10^{-13}	–	–	–
	r_{corner} = 15	5.68×10^{-12}	–	–	–
p = 50	r_{corner} = 20	1.19×10^{-12}	8.26×10^{-12}	1.19×10^{-6}	7.66×10^{-7}
	r_{corner} = 25	7.76×10^{-13}	–	–	–

Note: Empty cells represent combinations that were not part of the sensitivity study.

4.3.2 Combined probability of initiation of crack growth

As stated in Section 2.7, the defect distribution developed by JRC /14/ assumes the existence of one crack-like defect, and the size of this defect is characterised by an exponential distribution. The probabilistic analysis in Section 4.3.1 therefore calculates the probability of initiation of crack growth due to a single crack.

Using the analysis above, it is possible to calculate the combined probability of initiation of crack growth using a slice of the insert (along a path as defined by Figure 3-11). The thickness of the slice could be roughly assumed to be equal to diameter of the tensile specimen used to derive the defect distribution (d = 14 mm). Along the entire length of the insert (L = 4,573 mm), a number of such slices may be considered ($n = L/d$ = 327). However, in the analysis we have only considered one of eight possible positions in the insert (because of the symmetry of the insert). Therefore, the number of slices should be equal to $n = 8\times327 = 2{,}616$.

Assuming statistical independence, the combined probability of initiation of crack growth will be

$$P_{initiation}^{combined} = 1-\left(1-P_{initiation}\right)^{n} \approx n\cdot P_{initiation} \quad , \tag{4.12}$$

the latter since $P_{initiation} << 1$.

The combined probability of initiation of crack growth are presented in Table 4-3 (using n = 2,616).

The combined probability of initiation of crack growth is therefore estimated to be $P_{initiation}^{combined} = 1.98\times10^{-9}$ (for the baseline case using p = 44 MPa, r_{corner} = 20 mm, $\delta_{cassette}$ = 0 mm).

Table 4-3. The combined probability of initiation of crack growth when p = 40–50 MPa. Results using r_{corner} = 15–25 mm, $\delta_{cassette}$ = 0–15 mm and μ_a = 1.9 mm.

		$\delta_{cassette}$ = 0	$\delta_{cassette}$ = 5	$\delta_{cassette}$ = 10	$\delta_{cassette}$ = 15
	r_{corner} = 15	2.22×10^{-9}	–	–	–
p = 40	r_{corner} = 20	2.01×10^{-9}	2.05×10^{-9}	1.24×10^{-8}	4.81×10^{-5}
	r_{corner} = 25	2.05×10^{-9}	–	–	–
	r_{corner} = 15	2.72×10^{-9}	–	–	–
p = 44	r_{corner} = 20	1.98×10^{-9}	2.04×10^{-9}	6.17×10^{-7}	1.78×10^{-3}
	r_{corner} = 25	2.16×10^{-9}	–	–	–
	r_{corner} = 15	2.88×10^{-9}	–	–	–
p = 45	r_{corner} = 20	1.99×10^{-9}	2.04×10^{-9}	1.67×10^{-6}	4.42×10^{-3}
	r_{corner} = 25	2.19×10^{-9}	–	–	–
	r_{corner} = 15	1.49×10^{-8}	–	–	–
p = 50	r_{corner} = 20	3.11×10^{-9}	2.16×10^{-8}	3.11×10^{-3}	2.00×10^{-3}
	r_{corner} = 25	2.03×10^{-9}	–	–	–

Note: Empty cells represent combinations that were not part of the sensitivity study.

4.4 Probability of failure of the canister insert

When evaluating the probability of failure of the canister insert, we have to compare the results from Section 4.2–4.3 and see what failure mechanism that is dominating. This comparison is presented in Figure 4-9 (using the assumptions regarding a combined probability of initiation of crack growth as presented in Section 4.3.2).

Obviously, the initiation event dominates when the external pressure is below the baseline case ($p \approx 44$ MPa). Also the collapse event is strongly dependent of the assumed external pressure. The reason for this strong dependence is related to the pressure value at onset of local plastic collapse, if $\delta_{cassette} = 0$ mm then collapse starts at $p \approx 50$ MPa, if $\delta_{cassette} = 15$ mm then collapse starts at $p \approx 40$ MPa (see Figure 4-10). Since the baseline pressure is 44 MPa (i.e. between 40 and 50 MPa), then small deviations in the input data will produce large variations in the calculated probabilities of local collapse.

It has to be remembered that the analysis of collapse only considers the first local collapse event, total collapse of the insert will occur at a much higher pressure. If one conducts a full collapse finite element analysis of the insert (using a complete stress-strain curve /9/) the collapse pressure are calculated to be (see Figure 4-11):

- p_{max} = 104 MPa (only the pressure-bearing insert of nodular iron was included in the model).
- p_{max} = 118 MPa (the outer corrosion barrier made of copper was also included).
- p_{max} = 130 MPa (estimate for the case when both the steel cassette and the corrosion barrier was included in the model).

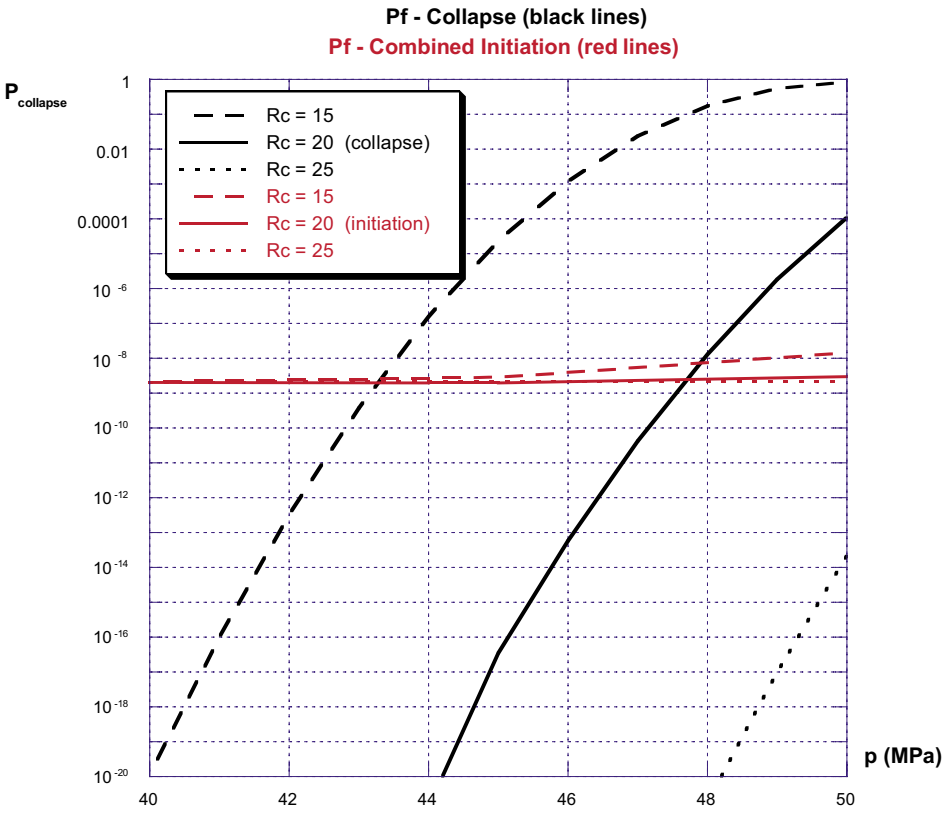

Figure 4-9. *Probability of failure when p = 40–50 MPa. Results using r_{corner} = 15–25 mm, $\delta_{cassette}$ = 0 mm, μ_a = 1.9 mm.*

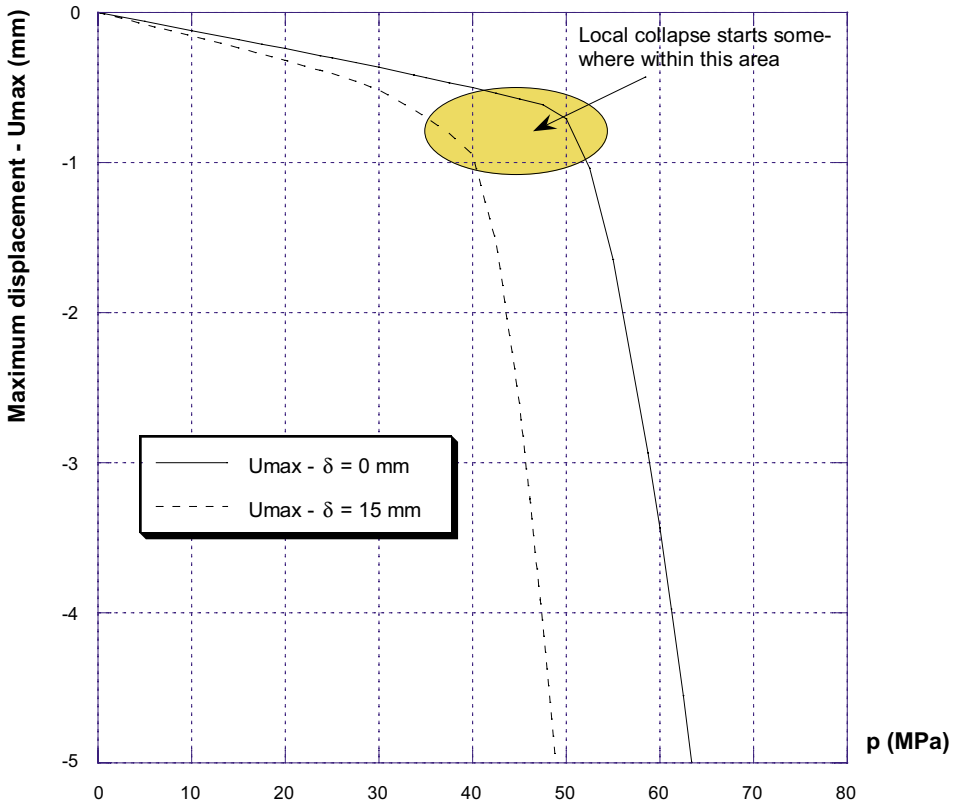

Figure 4-10. *Load-displacement curve, results using r_{corner} = 20 mm, $\delta_{cassette}$ = 0–15 mm.*

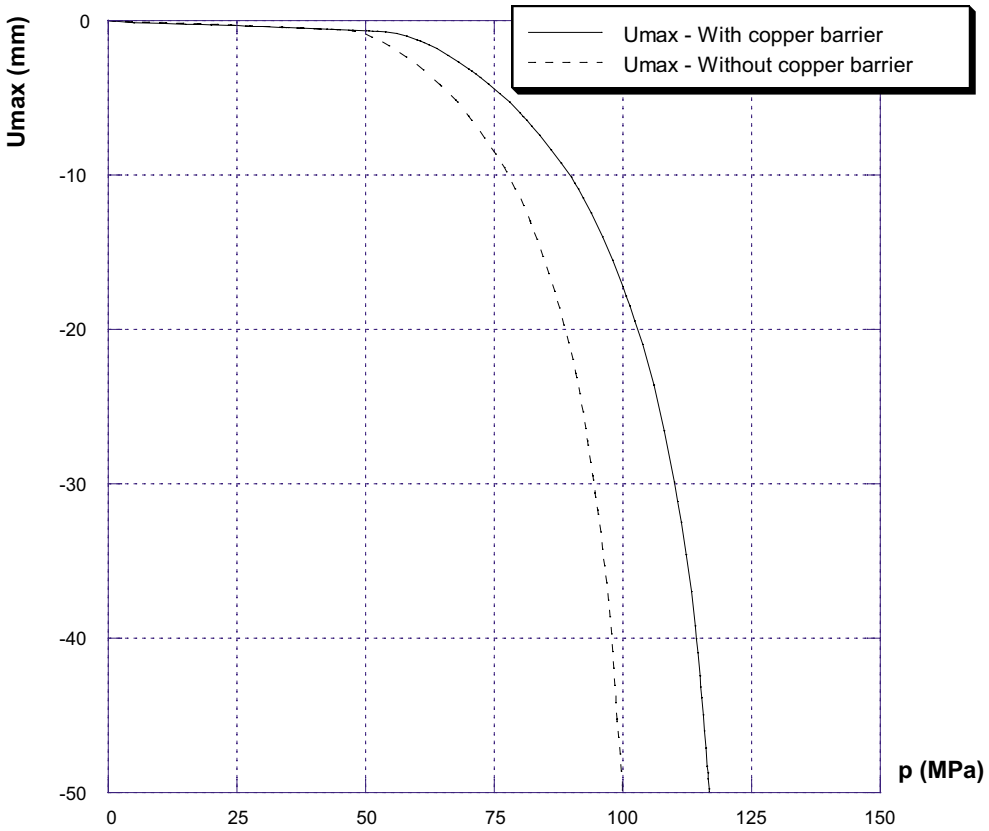

Figure 4-11. *Load-displacement curve, results using r_{corner} = 20 mm, $\delta_{cassette}$ = 0 mm.*

5 Conclusions

In this study, probabilistic analysis of canister inserts for spent nuclear fuel has been performed. The main conclusions are:

1. For the baseline case, the probability of failure is insignificant ($\sim 2\times10^{-9}$). This is the case even though several conservative assumptions have been made both in underlying deterministic analysis and in the probabilistic analysis.
2. The initiation event dominates (over the local collapse event) when the external pressure is below the baseline case (p = 44 MPa). The local collapse event dominates when the external pressure is above the baseline case (the two events are equal when $p \approx$ 47.5 MPa).
3. The local collapse event is strongly dependent of the assumed external pressure.
4. The analysis of collapse only considers the first local collapse event; total collapse of the insert will occur at a much higher pressure.
5. The resulting probabilities are more dependent on the assumption regarding the eccentricity of the cassette than the assumption regarding outer corner radius of the profiles for steel section cassette. The results indicate that the maximum allowed eccentricity should not be larger than 5 mm.
6. The probability of initiation of crack growth is calculated using a defect distribution where one assumes the existence of one crack-like defect. A simple scaling argument can be applied to consider the number of defects through the thickness.

6 References

/1/ **Öberg H, 2003.** Fracture toughness testing of nodular cast iron, Report SKB0304rep, Department of Solid Mechanics, KTH. Appended to ref /4/.

/2/ **Öberg H, 2004.** Fracture toughness testing of nodular cast iron, I24 and I25, Report SKB0401rep, Department of Solid Mechanics, KTH. Appended to ref /4/.

/3/ **Minnebo P, 2005.** Fracture Properties of Ductile Cast Iron used for Thick-Walled Components, Euro Report EUR21841EN to be published, Joint Research Centre of the European Commission.

/4/ **Nilsson K-F et al. 2005.** Probabilistic analysis and material characterisation of canister insert for spent nuclear fuel – summary report, SKB TR-05-17, Svensk Kärnbränslehantering AB.

/5/ **Minnebo P, 2003.** Tensile Experiments performed on Canister Insert I26, Interim Report NSU/PM/0308.001, Vers. 1, Joint Research Centre of the European Commission.

/6/ **Dillström P et al. 2004.** A combined deterministic and probabilistic procedure for safety assessment of components with cracks – handbook, DNV Research Report 2004/01, Rev. 4-1, Det Norske Veritas AB.

/7/ **Minnebo P, 2004.** Statistical Analysis of Engineering Tenslie Properties of Canister Insert Material, Interim Report TN.P.04.100, Vers. 1, Joint Research Centre of the European Commission.

/8/ **Mattson A, 2003.** Kompressionsprov av Gjutjärnskutsar enligt ASTM E9, Reg. nr. 16/51/14497, Kockums AB. (In Swedish).

/9/ **Minnebo P, Mendes J, 2004.** Compression Experiments addressing Canister Inserts I24 and I25, Interim Report NSU/PM/0408.001, Vers. 1, Joint Research Centre of the European Commission.

/10/ **ANSYS, 2003.** Release 8.0A01, Update 20031124, ANSYS Inc.

/11/ **ANSYS, 2005.** Release 9.0A1, Update 20050128, ANSYS Inc.

/12/ **BWR Serial 2, Steel Profile Cassette, Copper/Iron Canister, 2000.** Drawing Nr. 00014-121, Rev. A, Svensk Kärnbränslehantering AB.

/13/ **Nilsson K-F et al. 2005.** Pressure Tests of two KBS-3 Canister Mock-Ups. SKB TR-05-18, Svensk Kärnbränslehantering AB.

/14/ **Nilsson K-F, Blagoeva D, 2005.** Probabilistic model to correlate elongation to defects in cast iron for nuclear waste, Submitted to *Engineering Fracture Mechanics*.

/15/ **Erixon B, 2004.** Hållfasthetsanalyser inom probabilitisk analys av kapselhållfasthet, ÅF-S Report B794, ÅF-System AB. Appended to ref /4/.

ISSN 1404-0344
CM Digitaltryck AB, Bromma, 2005